JOURNAL OF Applied Polymer SCIENCE

Effect of nanofiller on the behavior of a melt-drawn HDPE/PA6 microfibrillar composite

Ivan Kelnar,[1] Ludmila Kaprálková,[1] Jaroslav Kratochvíl,[1] Jiří Kotek,[1] Libor Kobera,[1] Jakub Rotrekl,[2] Jiřina Hromádková[1]

[1]Institute of Macromolecular Chemistry, Academy of Sciences of the Czech Republic, Heyrovského nám. 2, 162 06 Praha, Czech Republic

[2]Faculty of Chemical Technology, University of Pardubice, Studentská 95, 532 10 Pardubice 2, Czech Republic

Correspondence to: I. Kelnar (E-mail: kelnar@imc.cas.cz)

ABSTRACT: Microfibrillar composites (MFCs) with reinforcing fibrils formed *in situ* by melt drawing were modified by the addition of layered silicates using different mixing protocols, *viz* simultaneous addition of components, application of respective premade nanocomposites and their combinations. The objective was to combine reinforcement with changes in the final structure, especially the fibril dimensions. The presented results indicate good potential of the nanoclay to enhance the MFC based on the melt-drawn HDPE/PA6 system. The best mechanical behavior was achieved with the simultaneous addition of all components. The majority of the nanofiller material was contained inside the PA6 fibrils. Both fibrils dimensions and mechanical behavior were significantly affected by the nanofiller migration to the PA6 phase in the course of mixing and melt drawing. Due to a complex effect of the clay, deterioration of mechanical properties was also found. As a result, numerous, in some cases contradictory, effects of nanofillers must be perfectly harmonized to improve the properties of MFCs. © 2014 Wiley Periodicals, Inc. J. Appl. Polym. Sci. **2015**, *132*, 41868.

KEYWORDS: clay; composites; mechanical properties; morphology

Received 2 September 2014; accepted 12 December 2014
DOI: 10.1002/app.41868

INTRODUCTION

Cold or melt drawing of extruded blends, preferably in the form of bristles or ribbons, is an advantageous method of preparing polymer-polymer composites.[1–15] In an optimal system, the *in situ* fiber (fibril)-forming phase consists of a semicrystalline polymer.[1–15] In this case, the processing temperature of the matrix is sufficiently lower than the melting temperature of the *in situ* formed fibrils, and microfibrillar composites (MFCs) can be subsequently processed using conventional methods, similar to short fiber composites with inorganic reinforcement. Most of these microfibrillar composites prepared using either cold- or melt-drawing methods are based on a polyolefinic matrix with polyethylene terephthalate (PET) or polyamide inclusions. When a continuous kneader is used for blending and subsequent extrusion, a short polymer fiber composite can be prepared in one simple processing unit. In the case of melt-drawing process,[8–12] the extruder must be combined with a cooling bath and a simple take-up device (rolls). The process can also benefit from using a special, for example, a slit or channel die providing convergent flow to form elongated inclusions.[13–15] For cold drawing, usually, a set of two take-up rolls is required, together with control of temperature of the extruded filament.[1–7]

In spite of many advantages of MFCs, such as zero wear of the processing equipment, good recyclability, and low density, MFCs possess limitations of poor mechanical properties and poor dimensional stability at elevated temperatures. Both these parameters can be improved by nanofillers (NFs), which may, in some cases, even support drawability.[16]

Of importance is also the well known structure-directing effect of NFs in a multicomponent system, i.e. influencing of dynamic phase behavior.[17–21] This influence consists in affecting many parameters, such as interfacial tension, viscosity ratio, and coalescence.

In the area of MFC modification using nanofillers, the effort has primarily been focused on conductive systems incorporating carbon black (CB)[22,23] and carbon nanotubes (CNTs)[24,25] with the goal to form a percolated network of conductive fibrils containing CB or CNTs. In the case of CNTs in a PE/PET melt-drawn system, improvement of mechanical properties at very low (<0.75%) CNT contents was found, whereas with CNT content of over 1%, the formation of fibrils with a lower aspect ratio was observed.[24] Similarly, the incorporation of TiO_2 particles[26,27] was not beneficial for the improvement of mechanical properties due to negative effects on the fibril parameters. In

the studies of Denchev, many affecting structural parameters of PE/PA6 MFC in the presence of organophilized montmorillonite (oMMT) were described, but without the evaluation of macromechanical behavior.[28,29]

On the other hand, in the case of PP/PA6-containing oMMT, good fibril formation was observed up to 3.5% content, whereas 10% content had a detrimental effect.[30] The authors performed only ribbon extrusion without evaluation of mechanical behavior. The fibril formation was found upon addition of the PA6 nanocomposite instead of neat PA6 into PET and PC matrices;[31] however, these systems cannot be processed by conventional methods due to similar melting/processing temperatures of the components.

A positive effect of nanofillers on mechanical behavior was also demonstrated in the case of fibers with a blend-based matrix.[32,33] Though many excellent works regarding characterization of High-density polyethylene (HDPE(and PA6 components, related MFC, and even nanofiller-containing MFCs have been performed, almost none of them is focused on interrelation between structure and resulting mechanical behavior; for example, Dencheva *et al*[34] studied cold-drawn systems processed by the compression molding in laboratory press only. To the best of our knowledge, no study describing the effect of layered silicates on the structure/property relationship in the melt-drawn MFC with the final treatment via melt-processing techniques, such as injection molding, has been reported.

This study addresses the potential of organophilized layered nanosilicate, montmorillonite (oMMT), to improve the melt-drawn MFC based on the combination of a HDPE matrix with PA6 microfibrils prepared by melt drawing and subsequent injection molding.

EXPERIMENTAL

Materials

High-density polyethylene (HDPE) HYA 800 (Exxon Mobil), polyamide 6 (PA6) Ultramid B5, $M_n \sim 42000$, Ultramid B4, $M_n \sim 33000$, Ultramid B3, $M_n \sim 18000$ (BASF), clays based on natural montmorillonite: Cloisite 15A (modified with dialkyldimethylammonium chloride 95 meq/100 g) (C15), Cloisite 30B (modified with alkylbis(2-hydroxyethyl)dimethylammonium chloride 90 meq/100 g, with alkyl derived from tallow) (C30), (Southern Clay Products, Inc.)

MFC Preparation

Prior to mixing, PA6 and clay were dried at 85°C and 70°C, respectively, for 12 h in a vacuum oven. The mixing was carried out in a counter-rotating segmented twin-screw extruder (L/D 40) Brabender TSE 20 at 400 rpm, and temperatures of the respective zones of 230, 235, 240, 245, 245, and 250°C. The extruded bristle was melt-drawn using an adjustable take-up device. The draw ratio is the ratio between the velocity of the take-up rolls and the initial velocity of the extruded bristle. Dog-bone specimens (gauge length 40 mm) were prepared in a laboratory micro-injection molding machine (DSM). The barrel and the mold temperature was 200°C and was 70°C, respectively.

Clay addition protocols can be added as follows: (a) simultaneously with other components (b) application of premade PA6 nanocomposite (prepared in extruder, temperatures 260, 260, 260, 260, 260, and 265°C) (c) application of HDPE nanocomposite (temperature of all zones 200°C) (d) combination of (a) and (b).

Testing

Tensile tests were carried out using an Instron 5800 apparatus at 22°C and crosshead speed of 20 mm min^{-1}. At least eight specimens were tested for each sample. Young's modulus (E), maximum stress (σ_m), and elongation at break (ε_b) were evaluated; the corresponding variation coefficients did not exceed 10%, 2%, and 20%, respectively.

Tensile impact strength, a_t, was measured on one-side notched specimens using a Zwick hammer with energy of 4 J (variation coefficient 10–15%). The reported values are averages of 12 individual measurements.

Dynamic mechanical analysis (DMA) was performed in single-cantilever mode using a DMA DX04T apparatus at 1 Hz and heating rate of 1°C.min^{-1} from −120 to 250°C.

The differential scanning calorimetry (DSC) analysis was carried out using a Perkin-Elmer 8500 DSC apparatus. Samples of 5–10 mg were heated from 50°C to 250°C at the heating rate of 10°C min^{-1}. The melting temperature T_m was identified as the melting endotherm maximum. The crystallinity was calculated using the values 292.5 and 230.0 J.g^{-1} for the heat of melting of 100%crystalline HDPE and PA 6, respectively

Characterization of Structure

The structure of the fibrils was examined using scanning electron microscopy (SEM) with a Vega (Tescan) microscope); the HDPE matrix was removed using a Soxhlet extraction apparatus with boiling xylene for 10 h. For the transmission electron microscope (Tecnai) observations, ultrathin (60 nm) sections were prepared under liquid nitrogen using an Ultracut UCT (Leica) ultramicrotome. Due to use of drawn fibrils (in order to obtain thin-layer samples along fibrils length), the HDPE phase structure does not correspond to that of the injection molded samples used for mechanical testing; the objective of this observation was to evaluate clay localization only.

Wide-angle X-ray scattering (WAXS) experiments were performed using a pinhole camera (Molecular Metrology System, Rigaku, Japan) attached to a microfocused X-ray beam generator (Osmic MicroMax 002) operating at 45 kV and 0.66 mA (30 W). The camera was equipped with removable and interchangeable Imaging Plate 23 × 25 cm (Fujifilm). Experimental set-up covered the momentum transfer (q) range of 0.25–3.5 $Å^{-1}$. $q=(4\pi/\lambda)\sin\theta$, where $\lambda=1.54$ Å is the wavelength and 2θ is the scattering angle. Calibrations of the center and sample-to-detector distance were made using silicon (Si) powder. Samples were measured in transmission mode.

The aim was to observe differences in crystallinity and orientation from azimuthal scan.

Solid-State NMR Spectroscopy

The ^{13}C CP/MAS NMR spectra were recorded using a Bruker AVANCE III HD spectrometer (Larmor frequencies $\nu^{13}C = 125.783$ MHz) with a 4-mm MAS probe. Spinning speed of the

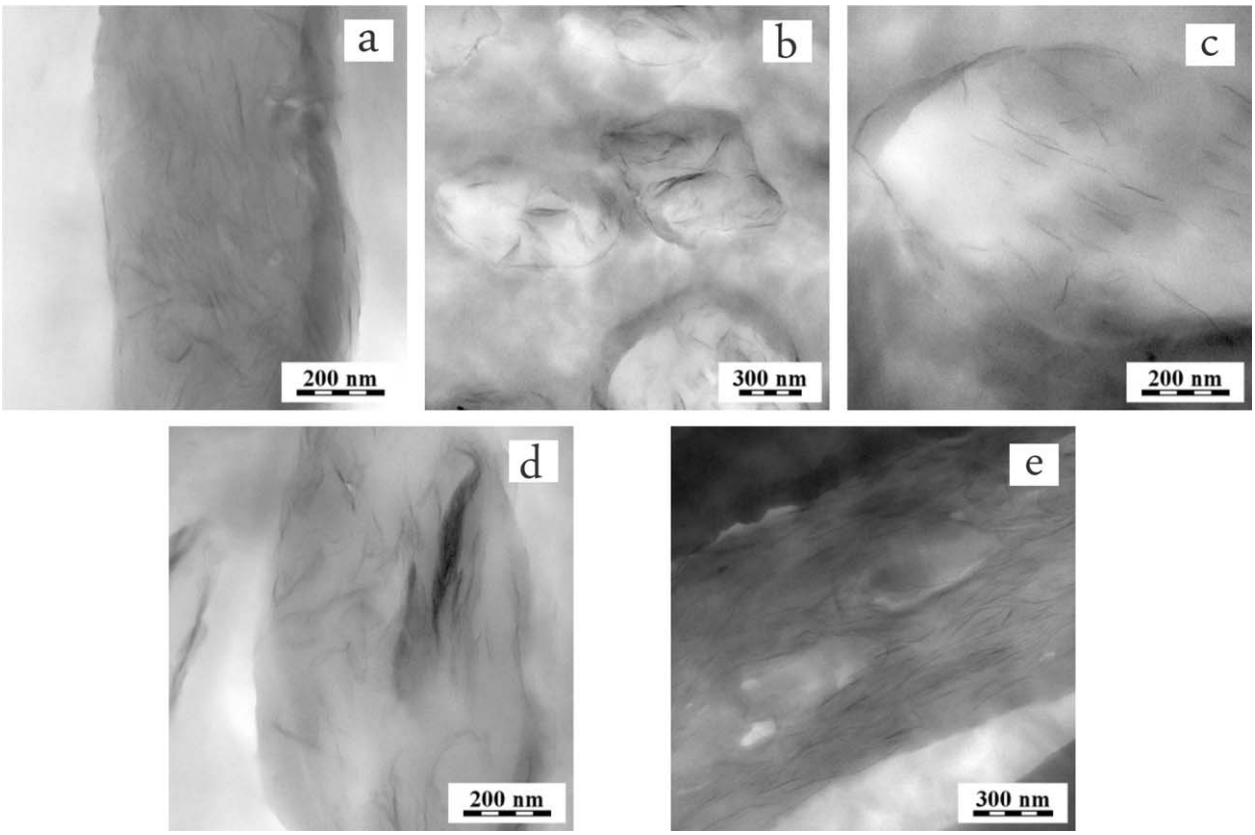

Figure 1. TEM images of HDPE/PA6 MFC containing: (a) 3% C30B; (b) 3% C15; (c) premade PA6/1% C15; (d) premade HDPE 3% C15; (e) premade HDPE/3% C30. Draw ratio = 7.

rotor sample was 11 kHz. The number of scans for the accumulation of the ^{13}C CP/MAS NMR spectra was 2048, the repetition delay was 4 s, and the spin lock was 2 ms. During detection, the high-power dipolar decoupling (SPINAL 64) was used to eliminate strong heteronuclear dipolar couplings. The isotropic chemical shift of the ^{13}C NMR scale was calibrated with glycine as an external standard (176.03 ppm to the carbonyl signal). In all cases, the dried samples were placed into the ZrO_2 rotors; all NMR experiments were performed at 303 K. The temperature calibration was performed on $Pb(NO_3)_2$ using a procedure described in the literature.[35]

RESULTS AND DISCUSSION

Effect of Clay Modification and Addition Protocol on the Fibril Parameters

The layered silicates, Cloisite C 30B (C30) and Cloisite 15A (C15), were added either simultaneously with mixing of both polymeric components, that is, HDPE and PA6 in the 80/20 w/w ratio, or in the form of premade PA6/oMMT nanocomposite (NC) or analogous HDPE/oMMT NC. TEM observations (Figure 1a) indicate that for C30 with relatively high affinity to PA6, confirmed by low value of corresponding interfacial energy[36] (especially in comparison with significantly higher value for PA6/C15) in Table I, the clay is in all cases (addition protocols) localized predominantly inside the PA6 fibrils. This localization is in agreement with published results,[39,40] both thermodynamic and kinetic factors[41] are favorable for the dominant migration of clay from HDPE to PA6. This occurs in spite of the fact that, due to lower melting temperature, majority of oMMT should be contained in HDPE at the early stage of mixing in case of one-step clay addition. Moreover, localization of C30 exclusively in the PA6 phase (fibrils) of the MFC is further supported by shear induced movement of oMMT[42] in the course of melt drawing.

C 15 was also found to be localized inside the PA6 phase; however, a more significant was its presence at the interface and in the HDPE phase [Figure 1(b,c)]. This is markedly documented in the case of addition of the premade HDPE/C15 nanocomposite (Figure 1d). The reason is higher interfacial energy of PA6/C15 (comparable with the HDPE/C15) (Table I), which is also

Table I. Interfacial Energies at Temperature 240°C

Systems	Interfacial energy[a] ($mJ.m^{-2}$)	Interfacial energy[b] ($mJ.m^{-2}$)
PA6/C30	1.79	0.8
PA6/C15	5	2.51
HDPE/C30	7.55	7.52
HDPE/C15	5.5	5.43

Calculated using harmonic[a] and geometric[b] mean equations[37], surface energy values, and their dispersive and polar components[38] were extrapolated to values corresponding to 240°C using the temperature coefficient.

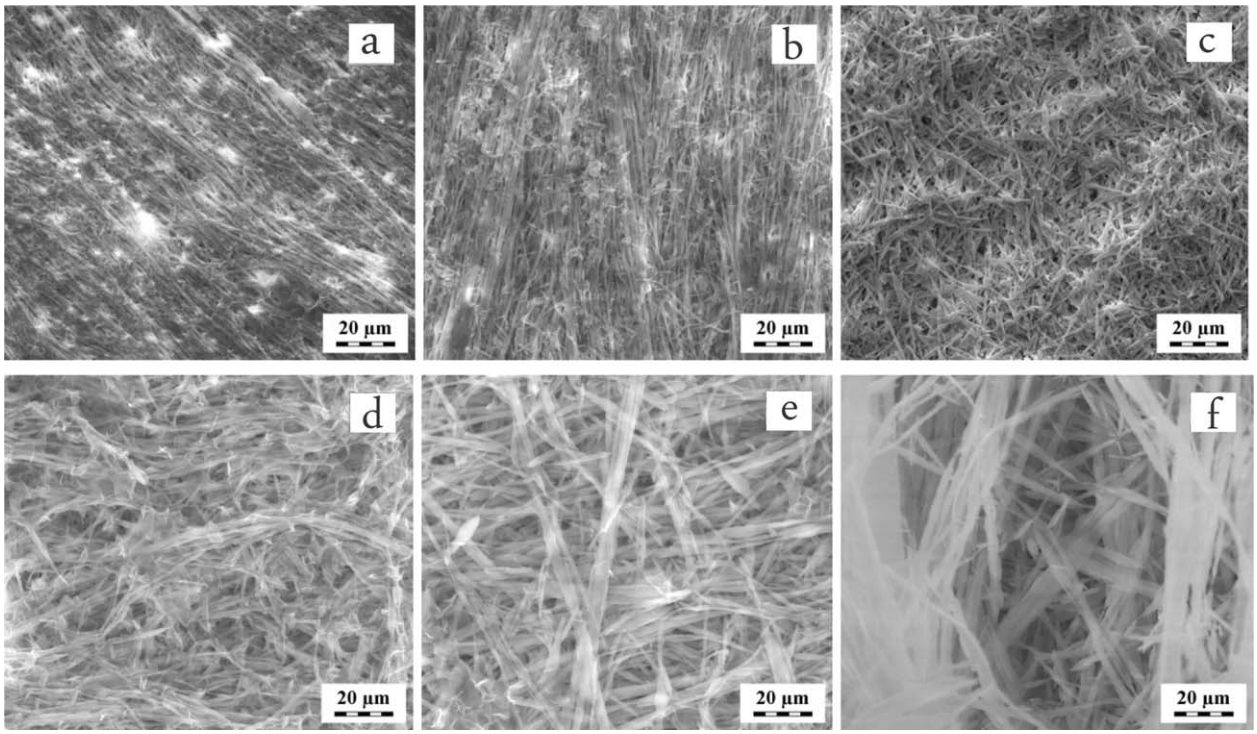

Figure 2. SEM images of PA6 fibrils in extracted HDPE/PA6 MFC containing: (a) no clay; (b) premade PA6/0.5% C30; (c) premade PA6/1% C30; (d) premade HDPE/3% C15; (e) HDPE/3% C30; (f) 3% C30. Draw ratio = 7.

responsible for the apparent lower degree of exfoliation found by TEM. Moreover, clay localization and transfer between phases is also influenced by other factors, namely by viscosity.[36]

With the premade HDPE/C30 NC, the remarkable presence of entrapped HDPE inclusions inside the PA6 fibrils was also observed (Figure 1e). This structure seems to be a consequence of the "coalescence-aided" formation of fibrils.

On the contrary, in spite of the similar final predominant localization of oMMT inside the PA6 fibrils, oMMT addition method strongly influences the shape and dimensions of the fibrils (Figure 2). As a result, oMMTs containing MFCs differ in the increase in the fibril diameter and the corresponding decrease in the aspect ratio.

From Figure 2a, the diameter of fibrils in neat MFC is ~1 μm, with an aspect ratio >100. Application of the premade PA6/C30 nanocomposite leads to the least marked increase in the fibril diameter (Figure 2b) which is slightly more marked with higher clay content; this effect is more pronounced in the case of premade PA6/C15 NC addition. The fibrils were also formed with the pre-made PA6/C30 NC with high (10%) clay content (not shown). This result indicates a low hindering effect of clay on the melt drawing of the PA6 phase. A relatively insignificant increase in diameter (~1.1 μm) was also found in the case of the HDPE nanocomposite containing 3% C 15 (Figure 2d). On the contrary, in the case of HDPE/C30B NC, more marked increase in diameter (<3 μm) and even irregular shapes (varying diameter along the fiber length) occurred (Figure 2e). Moreover, in the case of HDPE/C30 NC, the effect of clay on fibril formation led to the above-mentioned HDPE subinclusions formation inside PA6 fibrils. Finally, the most significant increase in diameter (ranging between 3–10 μm) was found for the MFC formed with the simultaneous addition of C30 (Figure 2f); for the analogous MFC containing C15, this effect was less marked.

These results indicate that formation of fibrils is significantly influenced by oMMT migration to the PA6 phase (more significant for C30) in the course of mixing and melt drawing of MFC. This influence most likely causes different changes in rheological parameters during this process. The results obtained indicate that an obviously more intensive (faster) migration of C30 in comparison with C15 (indicated by the presence of a greater amount of clay inside the fibrils and higher exfoliation in Figure 1) results in a greater diameter of the fibrils. We tentatively consider different effects of migration of finely dispersed C30, including its possible disordering due to passing through the interface[43] in comparison with C15 showing lower degree of dispersion.

For two PA6 types with lower molecular weight, the fibrils formed in neat MFC were shorter with slightly increased diameter, that is, in this HDPE/PA6 system, a higher viscosity ratio (dispersed phase/matrix) is favorable to form finer fibrils. At the same time, the effect of added clay on dimensions of the fibrils was comparable with that of the high molecular weight polyamide-based MFC.

From Figure 2, the admixing of additional C30 into the sample with the premade PA6 nanocomposite obviously leads to a

Table II. Mechanical Properties of HDPE/PA6 (80/20w/w) in Dependence on the Amount of Simultaneously Added Clay

Sample composition	Draw ratio	Max. stress (MPa)	Break strain (%)	E Modulus (MPa)	Toughness (kJ.m^{-2})
HDPE	0	35 ± 1.3	52 ± 9	1120 ± 110	25 ± 2.1
HDPE/PA6	0	44 ± 2.1	5.5 ± 2.6	1400 ± 165	21 ± 2
HDPE/PA6 (250°C)[a]	0	26 ± 1.1	7 ± 0.8	1300 ± 82	-
HDPA/PA6	7	45 ± 2	8.5 ± 1	1520 ± 103	20.5 ± 3.2
HDPE/PA6/1%C30	0	44 ± 1.6	8 ± 1	1575 ± 88	22 ± 1.8
HDPE/PA6/1%C30	7	46 ± 3	8 ± 0.8	1600 ± 98	21 ± 3.8
HDPE/PA6/2%C30	0	45 ± 2.4	8 ± 0.5	1600 ±± 55	30 ± 8
HDPE/PA6/2%C30	7	48 ± 3	9 ± 0.7	1700 ± 62	35 ± 5
HDPE/PA6/3%C30	0	35 ± 2.1	10 ± 0.9	1500 ± 70	12 ± 3.1
HDPE/PA6/3%C30	7	46 ± 2	7.5 ± 1	1850 ± 105	18 ± 2.6
HDPE/PA6/5%C30	0	33 ± 1.9	9 ± 0.7	1490 ± 80	14 ± 2.7
HDPE/PA6/5%C30	7	35 ± 2.4	8 ± 0.7	1580 ± 75	19 ± 2.5
HDPE/PA6/3%C15	0	36 ± 1.9	10 ± 1	1450 ± 53	20.7 ± 2.4
HDPE/PA6/3%C15	7	40.5 ± 2	8.5 ± 0.9	1530 ± 62	27 ± 2.5

[a] Sample injection molded at temperature exceeding the melting point of PA6.

significant increase in diameter of the fibrils. This increase is less marked in comparison with the analogous MFC with neat PA6 but leads to a more significant irregular shape of fibrils. Possible explanation is hindering of migration of clay between the components due to the presence of the premixed oMMT inside PA6. This result also confirms a marked effect of clay migration on fibril formation in the course of melt drawing. Another effect is the change in the initial rheological properties of the PA6 phase due to the premixed clay. Because the initial (undrawn) blend contains PA6 particles of ~2.3 μm in size which was reduced to below 2 μm in all clay-containing systems, more voluminous fibrils must be formed by coalescence of these inclusions in the course of melt drawing.[10,44,45] The increase in size of the fibrils by addition of oMMT is contradictory to the effect in the undrawn system. Explanation of the effect of oMMT on the melt-drawn fibrils formation process, including the obvious importance of oMMT migration between phases, and the corresponding change of the rheological parameters is the subject of the associated rheological study.[45]

Effect of oMMT on Mechanical Properties

From Table II, the best mechanical behavior was clearly achieved in the case of the simultaneous addition of clay (together with polymeric components). A significant increase in the mechanical parameters occurred in the case of 2% and 3% clay addition. The best balanced behavior, that is, increased strength and stiffness accompanied by the highest value of toughness, was found for 2% content, whereas with 3% clay, a slightly higher modulus was accompanied by reduced toughness. Rather unexpected is the significant reduction of all parameters for the 5% clay addition because such a concentration dependence is in contradiction with that of one-phase and also many two-phase matrix (undrawn) nanocomposites.[17–21]

In the case of the undrawn blend, lower strength of the clay-containing system in comparison with analogous clay-free one (Table II) is caused by suppression of fibril formation in the former system during the passing through the die.

Note that the best mechanical parameters were found for MFCs with relatively rough fibrils of less favorable aspect ratio in comparison with all other composites prepared (Figure 2). At the same time, the fibril diameter <10 μm with length exceeding 100 μm are apparently within the optimal range, which leads to effective reinforcement in both inorganic and carbon fiber composites. Moreover, the relatively lower aspect ratio is less important because the role of the aspect ratio and adhesion is less pronounced due to less marked difference between the parameters of the matrix and fibers,[46] as clearly shown in Figure 3. In addition, long finer fibers may form less effective entanglements.[47] This result indicates the importance of fiber reinforcement by clay and parameters of the interface. However,

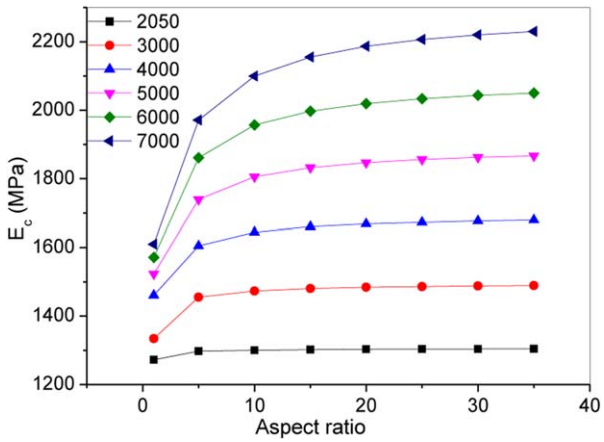

Figure 3. Effect of aspect ratio and modulus of fibers on the stiffness of MFCs; the numbers inside the chart indicate fiber modulus. The values were calculated using the Halpin–Tsai model.[46] [Color figure can be viewed in the online issue, which is available at wileyonlinelibrary.com.]

Table III. Mechanical Properties of HDPE/PA6 (80/20 w/w) in Dependence on the Composition of the Pre-Mixed Nanocomposite and the Simultaneously Added oMMT

Sample composition	Draw ratio	Max. stress (MPa)	Break strain (%)	E Modulus (MPa)	Toughness (kJ.m^{-2})
HDPE/(PA6 + 0.5% C30)[a]	6	44 ± 1.7	8 ± 0.7	1560 ± 90	25 ± 3.2
HDPE/(PA6 + 0.5%C30)[a]/3%C30	8	46 ± 1.9	8 ± 0.7	1780 ± 95	24 ± 2.8
HDPE/(PA6 + 1%C30)[a]	6	37 ± 1.6	11 ± 0.8	1430 ± 75	14 ± 3
HDPE/(PA6 + 1%C30)[d]/3%C15	7	33 ± 1.6	12 ± 0.9	1260 ± 95	15 ± 3.2
HDPE/(PA6 + 5%C30)[a]	6	37 ± 2	13 ± 1.1	1400 ± 65	20 ± 2
HDPE/(PA6 + 10%C30)[a]	8	39 ± 1.8	9 ± 0.7	1500 ± 105	15 ± 3
(HDPE + 3%C15)[b]/PA6	6	38 ± 2.5	9 ± 1	1550 ± 110	24 ± 1.6
(HDPE + 3%C30)[b]/PA6	6	41 ± 1.6	8 ± 0.5	1590 ± 85	29 ± 6
HDPE/(PA6 + 1%C15)[a]	7	32.5 ± 2	10 ± 0.9	1360 ± 80	20.5 ± 3

[a] Premade PA6 matrix nanocomposite.
[b] Premade HDPE nanocomposite.

mechanical properties impaired by higher clay content indicate different, more complex effects of clay on MFCs in comparison with the undrawn systems, including the effect of oMMT migration to the PA6 phase.

From Table III, the application of premade NCs with various oMMT contents is a less efficient method of the MFC modification. In this case, just PA6/C30 NC containing low 0.5% clay content leads to a slight improvement of mechanical properties that can be more improved by simultaneous admixing of additional C30. However, with the addition of NC containing 1% or more of C30, strength was particularly reduced in comparison with MFCs made by simultaneous clay addition (Table II). This phenomenon occurs in spite of the expected comparable reinforcement of fibrils because, except for the same dominant localization of clay inside fibrils, the premade NC composition approximately corresponds to the final content of oMMT in fibrils in the simultaneously mixed system (Table II). Even more unexpected is further decrease, especially of stiffness, when C15 clay with higher affinity to the HDPE matrix was added together with the PA6 nanocomposite. Moreover, this observation indicates different and more complex affecting of the studied systems, especially the interface with clay. At the same time, the content of crystalline phase of all samples is quite similar, with neither DSC (Table IV) nor XRD (Figure 4) indicating marked differences in the parameters evaluated. The peaks in Figure 4 represent the same orientation of fibrillar portion and small part of unoriented material as well. A similar decrease in modulus was observed in blends in spite of presence of the nanofiller;[48] no enhancement of stiffness and strength was found in PP/PA66 microfibrillar composite containing CNT.[25]

To explain the above-mentioned impairment of the mechanical behavior, we tentatively consider a crucial importance of the parameters of the fibrils and the interface.[49–52] The interface may be influenced by different crystalline-phase content (including the amorphous layer), its orientation, and type. This behavior could be influenced by the expected difference in clay localization and ordering at and near the interface, most probably caused by the above-mentioned clay migration to PA6. In spite of the expected great effect of the thin amorphous (low modulus) layer on stiffness decrease,[51,52] it has no detectable effect on the bulk crystallinity. Some changes of the interface were indicated by different density of PE spherulites near the fibril surface (Figure 5) observed by light microscopy (LM) of samples with different mechanical behavior. Unfortunately, the

Table IV. DSC Analysis of Microfibrillar Composites; Effect of oMMT and Drawing

	HDPE		PA 6		
	T_m (°C)	CR (%)	T_m (°C)	CR (%)	Content γ (%)
HDPE/PA6/3C30(0)	134.3	67.1	219.7	20.4	5
HDPE/PA6/3C30(7)	135.0	64.5	220.9	26.4	0
HDPE/(PA6/1C30)(0)	133.8	57.6	221.2	39.3	3
HDPE/(PA6/1C30)(7)	133.7	65.0	220.3	37.5	0
HDPE/(PA6/10C30)(8)	133.1	67.4	219.4	28.8	1
HDPE/(PA6/1C30)/3C15(0)	131.8	62.9	220.1	24.7	40
HDPE/(PA6/1C30)/3C15(7)	133.9	64.9	220.4	27.4	2
(HDPE/3C30)/PA6(6)	134.1	63.5	221.2	20.4	tr.

The numbers in the brackets represent the draw ratio.

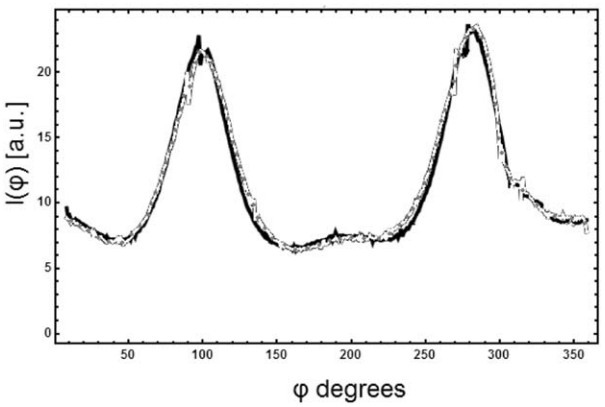

Figure 4. XRD patterns: HDPE/PA6/3%C30; HDPE/premade PA6/1%C30/3%C15. Draw ratio = 7.

observations are close to the resolution limit of LM due to the fine dimensions of HDPE spherulites. Differences in HDPE crystallinity were also found using NMR. The studies to explain the effect of clay on dynamics of the PA6 chains, including simulation of the impact of "soft" interface[51] parameters on behavior, are in progress.

Effect of Polyamide Chain Length on Mechanical Properties

Table V presents the behavior of analogous MFCs containing PA6 of different molecular weights. The improved mechanical properties are clearly observed for PA6 of relatively high molecular weight ~45000. With two types of PA6 of lower chain lengths, the mechanical parameters are significantly impaired in spite of the relatively comparable fibrils parameters. This result further confirms low importance of the fibril dimensions and the complex effect of oMMT on MFC behavior.

Dynamic Mechanical Analysis (DMA)

From Figure 6a, in the simultaneously mixed MFC sample, the glass transition temperature (T_g) of PA6 fibrils obviously increases with oMMT content, with a maximum at 3% C30 content and a decrease at 5%. This observation corresponds to impaired mechanical properties for this oMMT content and further confirms a complex effect of clay. The increase in T_g is slightly more marked for premade NC, with a decrease for the PA6 nanocomposite containing 10% of C30. In the case of undrawn blend, a slight reduction of T_g with increasing clay content was observed, that is, the result is in agreement with the effect of oMMT on T_g of a single NC.[53] Moreover, the existence of a "simple" T_g peak of PA6 in MFC represents another difference from the undrawn PA6 NC, where lowering of the "original peak" is accompanied by a shoulder at the high-temperature side.[53]

In most clay-containing MFCs, T_g increases with increasing draw ratio, and even more significantly with higher C30B content (up to 5%) as shown in Figure 6b; the only exception is a decrease for the MFC-containing premade PA6 NC with 10% C30. At the same time, the effect of draw ratio in neat MFC

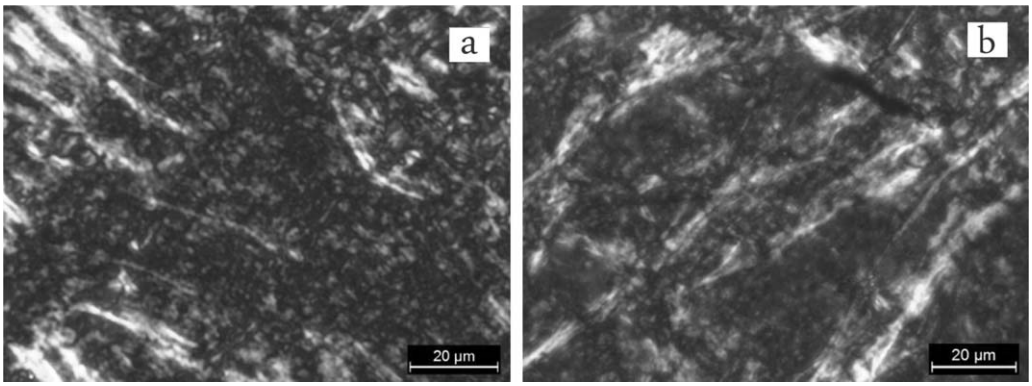

Figure 5. Polarized light microscopy images: (a) HDPE/premadePA6 1% C30/3% C15; (b) HDPE/PA6/3% C30. Draw ratio = 7.

Table V. Mechanical Properties of HDPE/PA6 (80/20 w/w) in Dependence on the PA6 Type, Draw Ratio 7

Sample composition	Max. stress (MPa)	Break strain (%)	E Modulus (MPa)	Toughness (kJ.m^{-2})
[a]HDPE/PA6/C30(3%)	46 ± 2	7.5 ± 1	1850 ± 105	18 ± 2.6
[b]HDPE/(PA6 + 1%C30)	37 ± 1.6	11 ± 1.1	1430 ± 95	14 ± 2.4
[a]HDPE/B4/[c]/C30(3%)	32 ± 1.7	8 ± 0.7	1510 ± 78	20 ± 3
[b]HDPE/(B4[c] + 1%C30)	37 ± 1.5	8.5 ± 0.8	1450 ± 82	20 ± 3.2
[a]HDPE/B3[d]/C30(3%)	32 ± 1.9	7 ± 1	1500 ± 71	15 ± 2.1
[a]HDPE/(B3[d] + 1%C30)	33 ± 2.2	9 ± 1.3	1320 ± 74	12 ± 2.3

[a] Simultaneous mixing of all components.
[b] C30 premixed with polyamide.
[c] Ultramid B4.
[d] Ultramid B3.

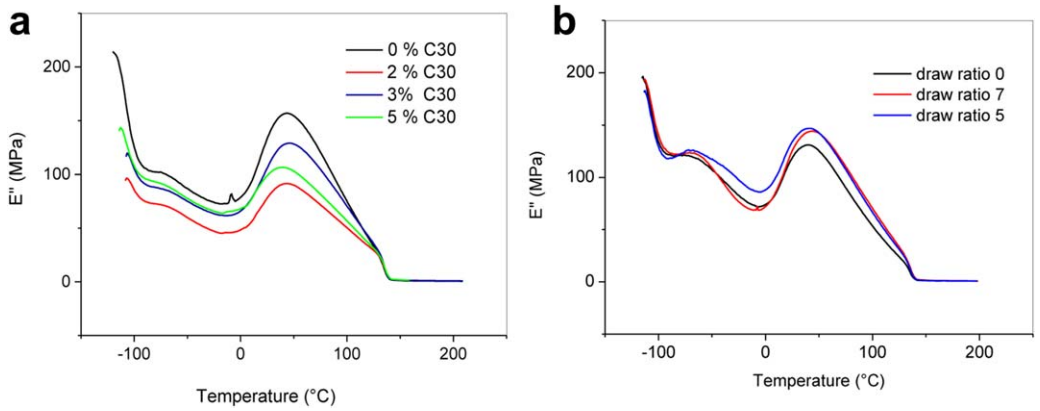

Figure 6. Temperature dependence of loss modulus of HDPE/PA6 MFC at: (a) various clay contents (draw ratio = 7); (b) various draw ratios (1% C30). [Color figure can be viewed in the online issue, which is available at wileyonlinelibrary.com.]

was insignificant. The increase in T_g is slightly lower for the analogous MFCs containing C15, most likely due to a lower exfoliation. T_g of HDPE/PA6 sample processed above the melting point of PA6 is even more reduced in comparison with the sample injection-molded without melting the PA6 phase; this indicates the above-mentioned certain drawing of PA6 inclusions during the passage through the extruder die.

From the DMA results, it is obvious that both the presence of oMMT and the higher extent of drawing increase T_g of PA6 fibrils, which undoubtedly contributes to a better dimensional stability of MFCs at elevated temperatures.

Solid-State NMR Evaluation

The ^{13}C CP/MAS NMR spectra of the prepared systems (Figure 7) clearly indicate the presence of multiple polymorphic forms of both polymer blocks. Specifically, the signals at 35 ppm, 32 ppm, and 30 ppm can be attributed to the monoclinic phase, the orthorhombic phase, and the amorphous phase of HDPE, respectively. Similarly, the resonances at 44 ppm and 39 ppm assigned to the CH_2 groups C1 reflect the alpha- and gamma-

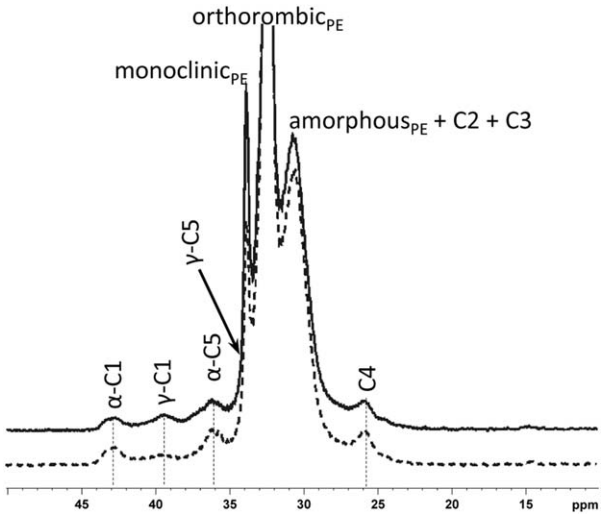

Figure 7. ^{13}C CP/MAS NMR spectra of HDPE/PA6 MFC: HDPE/PA6/3%C30; HDPE/premade PA6/1%C30/3%C15. Draw ratio = 7.

polymorphic form of PA6, respectively.[34,53] From the broadening of the carbonyl signal, the presence of the amorphous phase of PA6 can also be expected. The quantitative analysis of the recorded ^{13}C CP/MAS NMR spectra have revealed that the studied composites differ in the amount of the monoclinic phase of HDPE. In the simultaneously mixed MFC-containing 3% C30, approximately 10–15% of the monoclinic phase was found, which is more than that in MFC containing the premade PA6/1% C30 nanocomposite with the addition of 3% C15.

CONCLUSIONS

Application of oMMT in the melt-drawn microfibrillar HDPE/PA6 composites represents a means to improve their performance. The results indicate strong effect of different mixing protocols, that is, simultaneous addition of components, application of respective premade nanocomposites and their combinations, on the fibril dimensions and properties. This occurs in spite of the fact that most of oMMT is localized inside the PA6 fibrils for all mixing protocols; the best mechanical behavior was achieved with the simultaneous addition of all components. As a result, the mechanical behavior is influenced not only by fibril reinforcement but the effect of clay is more complex in comparison with the undrawn systems. The different course of oMMT migration into the PA6 phase during mixing and melt drawing is of crucial importance. This influences not only the corresponding changes in the viscosity ratio and interfacial tension but also the interfacial arrangement of oMMT. The last effect most likely determines the parameters of the interface which depend on the different type, content, and orientation of the crystalline phase of the material in this area and significantlyinfluence mechanical behavior of the composite. Consequently, the numerous effects induced by oMMT must be harmonized to achieve improved mechanical properties.

ACKNOWLEDGMENTS

This study was supported by Czech Science Foundation (Grant No 13-15255S). The authors would like to thank Dr. Borislav Angelov for the XRD analysis.

REFERENCES

1. Evstatiev, M.; Fakirov, S.; Friedrich, K. In Polymer Composites: From Nano- to Macro-scale; Friedrich, K.; Fakirov, S.; Zhang, Z., Eds.; Springer: New York, **2005**.
2. Fakirov, S.; Bhattacharyya, D.; Shields, R. *J. Colloid Surface A.* **2008**, *313*, 2.
3. Evstatiev, M.; Fakirov, S. *Polymer* **1992**, *33*, 877.
4. Shields, R. J.; Bhattacharyya, D.; Fakirov, S. *J. Mater. Sci.* **2008**, *43*, 6758.
5. Evstatiev, M.; Fakirov, S.; Krasteva, B.; Friedrich, K.; Covas, J.; Cunha, A. *Polym. Eng. Sci.* **2002**, *42*, 826.
6. Jayanarayanan, K.; Thomas, S.; Kuruvilla, J. *Compos. Part A-Appl. S.* **2008**, *39*, 164.
7. Sarkissova, M.; Harrats, C.; Groeninckx, G.; Thomas, S. *Compos. Part A-Appl. S.* **2004**, *35*, 489.
8. Pesneau, I.; Ait-Kadi, A.; Bousmina, M.; Michel, A.; Cassagnau, P. *Polym. Eng. Sci.* **2002**, *42*, 1990.
9. Boyaud, M. F.; Ait-Kadi, A.; Bousmina, M.; Michel, A.; Cassagnau, P. *Polymer* **2001**, *42*, 6515.
10. Huang, W. Y.; Shen, J. W.; Chen, X. M.; Chen, H. Y. *Polym. Int.* **2003**, *52*, 1131.
11. Lin, X. D.; Cheung, W. L. *J. Appl. Polym. Sci.* **2003**, *88*, 3100.
12. Wan, H. Q.; Ji, X. *J. Mater. Sci.* **2004**, *39*, 6839.
13. Li, Z. M.; Yang, M. B.; Xie, B. H.; Feng, J. M.; Huang, R. *Polym. Eng. Sci.* **2003**, *43*, 615.
14. Yi, X.; Xu, L.; Wang, Y. L.; Zhong, G. J.; Ji, X.; Li, Z. M. *Eur. Polym. J.* **2010**, *46*, 719.
15. Leung, K. K.; Easteal, A.; Bhattacharyya, D. *Compos. Part A-Appl. S.* **2008**, *39*, 662.
16. Fujiyama-Novak, J. H.; Cakmak, M. *Macromolecules* **2008**, *41*, 6444.
17. Lee, H.; Fasulo, P. D.; Rodgers, W. D.; Paul, D. R. *Polymer* **2005**, *46*, 11673.
18. Ray, S. S.; Pouliot, S.; Bousmina, M.; Utracki, L. A. *Polymer* **2004**, *45*, 8403.
19. Gelfer, M. Y.; Song, H. H.; Liu, L.; Hsiao, B. S.; Chu, B.; Rafailovich, M.; Si, M.; Zaitsev, V. *J. Polym. Sci. B-Polym. Phys.* **2003**, *41*, 44.
20. Kelnar, I.; Rotrekl, J.; Kaprálková, L.; Hromádková, J.; Strachota, A. *J. Appl. Polym. Sci.* **2012**, *125*, 3477.
21. Kelnar, I.; Khunová, V.; Kotek, J.; Kaprálková, L. *Polymer* **2007**, *48*, 5332.
22. Xu, X. B.; Li, Z. M.; Yang, M. B.; Jiang, S.; Huang, R. *Carbon* **2005**, *43*, 1479.
23. Dai, K.; Xu, X. B.; Li, Z. M. *Polymer* **2007**, *48*, 849.
24. Yesil, S.; Bayram, G. *J. Appl. Polym. Sci.* **2013**, *127*, 982.
25. Lin, R. J. T.; Bhattacharyya, D.; Fakirov, S. *Int. J. Mod. Phys. B.* **2010**, *24*, 2459.
26. Li, W. J.; Schlarb, A. K.; Evstatiev, M. *J. Appl. Polym. Sci.* **2009**, *113*, 1471.
27. Li, W. J.; Schlarb, A. K.; Evstatiev, M. *J. Appl. Polym. Sci.* **2009**, *113*, 3300.
28. Denchev, Z.; Dencheva, N.; Funari, S. S.; Motovilin, M.; Schubert, T.; Stribeck, N. *J. Polym. Sci. B: Polym. Phys.* **2010**, *48*, 237.
29. Dencheva, N.; Denchev, Z.; Stribeck, N.; Motovilin, M.; Zeinolebadi, A.; Funari, S. S.; Botta, S. *Macromol. Mater. Eng.* **2013**, *298*, 1100.
30. Feng, M.; Gong, F.; Zhao, C.; Chen, G.; Zhang, S.; Yan, M. *Polym. Inter.* **2004**, *53*, 1529.
31. Goitisolo, I.; Equizábal, J. I.; Nazábal, J. *Eur. Polym. J.* **2008**, *44*, 1978.
32. Bigdeli, A.; Nazockdast, H.; Rashidi, A.; Yazdanshenas, M. E. *Int. Polym. Proc.* **2013**, *28*, 174.
33. Heidari Golfazani, M. E.; Nazockdast, H.; Rashidi, A.; Yazdanshenas, E. *J. Macromol. Sci. B: Phys.* **2012**, *51*, 956.
34. Dencheva, N.; Oliveira, M. J.; Carneiro, O.; Nunes, T. G.; Denchev, Z. *Mater. Sci. Forum.* **2008**, *515*, 587.
35. Brus, J. *Solid. State. Nucl. Mag.* **2000**, *16*, 151.
36. Sumita, M.; Sakata, K.; Asai, S.; Miyasaka, K.; Nakagawa, H. *Polym. Bull.* **1991**, *25*, 265.
37. Wu, S. Polymer Interface and Adhesion, Marcel Dekker: New York, **1982**.
38. Taguet, A.; Cassagnau, P.; Lopez-Cuesta, J.-M. *Prog. Polym. Sci.* **2014**, *39*, 1526.
39. Filippone, D; Dintcheva, N. Tz.; Acierno, D.; La Mantia, F. P. *Polymer* **2008**, *49*, 1312.
40. Malmir, S.; Razavi Aghjeh, M. K.; Hemmati, M.; Ahmadi Tehrani, R. *J. Appl. Polym. Sci.* **2012**, *125*, E503.
41. Zonder, L.; McCarthy, S.; Rios, F.; Ophir, A.; Kenig, S. *Adv. Polym. Technol.* **2014**, *33*, 21427.
42. Elias, L.; Fenouillot, F.; Majesté, J. C.; Martin, G.; Cassagnau, P. *J. Polym. Sci. B: Polym. Phys.* **2008**, *46*, 1976.
43. Mi, D.; Liu, K.; Du, H.; Zhang, J. *Polym. Adv. Technol.* **2014**, *25*, 364.
44. Fakirov, S.; Bhattacharyya, D.; Lin, R. J. T.; Fuchs, C.; Friedrich, K. *J. Macromol. Sci. B: Phys.* **2007**, *46*, 183.
45. Kelnar, I.; Fortelný, I.; Kaprálková, L.; Hromádková, J. *Polym. Eng. Sci.* **2015**, DOI: 10.1002/pen.24055.
46. Halpin, J. C.; Kardos, J. L. *Polym. Eng. Sci.* **1976**, *16*, 344.
47. Samir, M.; Alloin, F.; Paillet, M.; Dufresne, A. *Macromolecules* **2004**, *37*, 4313.
48. Laoutid, F.; Estrada, E.; Michell, R. M.; Bonnaud, L.; Müller, A. J.; Dubois, P. *Polymer* **2013**, *54*, 3982.
49. Ville, J.; Médéric, P.; Huitric, J.; Thierry, A. *Polymer* **2012**, *53*, 1733.
50. Maurice, G.; Rouxel, D.; Vincent, B.; Hadji, R.; Schmitt, J. F.; Taghite, M.; Rahouadj, R. *Polym. Eng. Sci.* **2013**, *53*, 1502.
51. Ishida, H.; Chaisuwan, T. *Polym. Compos.* **2003**, *24*, 597.
52. Gerard, J. F. *Polym. Eng. Sci.* **1988**, *28*, 568.
53. Brus, J.; Urbanova, M.; Kelnar, I.; Kotek, J. *Macromolecules* **2006**, *39*, 5400.